J Polym Res (2015) 22: 205
DOI 10.1007/s10965-015-0839-7

ORIGINAL PAPER

Preparation and characterization of nano-hybrids combining poly(urea-imide) with a porous silica-pillared layered phase

Wei-Yao Chang [1] · Ching-Nan Chuang [1] · Szu-Hsien Chen [1] · Chih-Kuang Wang [2,3] · Kuo-Huang Hsieh [1,4]

Received: 11 June 2015 / Accepted: 10 September 2015 / Published online: 2 October 2015

Abstract The mechanical, thermal and dielectric properties of nano-hybrids comprised of poly(urea-imide) (PUI) and a highly porous nano-silica-pillared layered clay were studied. The PUI was prepared from an aromatic diamine (4,4′-diphenylmethane diisocyanate; MDI), an aromatic dianhydride (pyromellitic diahydride; PMDA) and 4,4′-oxydianiline (ODA). Different ratios of the nano-silica-pillared layered clays (NSP7030) were modified using tetraethoxysilane (TEOS) via a sol–gel process. The TEOS modified NSP7030 clays (NSP7030/TEOS) were further calcined at 500 °C (C-NSP7030/TEOS). The nano-hybrids comprised of PUI and C-NSP7030/TEOS clays were characterized by thermogravimetric analysis (TGA), scanning electron microscopy (SEM), and their mechanical and dielectrical properties et al. The results showed that the exfoliated (major) and intercalated (minor) structures of the nano-silica-pillared layered clays (NSP7030) were successfully modified by TEOS via a sol–gel process. Furthermore, the nano-hybrids exhibited slightly higher thermal stability than the pure PUI component. The highest thermal decomposition temperature at 5 % weight loss (T_d 5 %) of the material degraded was at 510 °C because the nano-hybrids contained poly(urea-imide) with 15 wt.% C-NSP7030/TEOS(1/5). Pure PUI exhibited good values of tensile strength and elongation which were 96.1 MPa and 9.0 %. After the addition of C-NSP7030/TEOS(1/5), the values of tensile strength and elongation decreased slightly. Surprisingly, the dielectric constant of nano-hybrids containing 15 wt.% C-NSP7030/TEOS(1/5) could be enhanced from 3.88 to 3.31. In addition, agglomerations of the C-NSP7030/TEOS(1/5) clay are observed in the micrographs when the PUI matrix was loaded with 10 and 15 wt% of the C-NSP7030/TEOS(1/5) clays.

Keywords Poly(urea-imide) · Silica-pillared · Nano-hybrids · Mechanical properties · Thermal properties

✉ Chih-Kuang Wang
ckwang@kmu.edu.tw

✉ Kuo-Huang Hsieh
khhsieh@ntu.edu.tw

[1] Institute of Polymer Science and Engineering, College of Engineering, National Taiwan University, No. 1, Sec. 4, Roosevelt Road, Taipei City 10617, Taiwan

[2] Department of Medicinal and Applied Chemistry, Kaohsiung Medical University, No. 100, Shih-Chuan 1st Road, Kaohsiung 80708, Taiwan

[3] Orthopaedic Research Center, Kaohsiung Medical University, No. 100, Shih-Chuan 1st Road, Kaohsiung 80708, Taiwan

[4] Department of Chemical Engineering, College of Engineering, National Taiwan University, No. 1, Sec. 4, Roosevelt Road, Taipei City 10617, Taiwan

Introduction

Nano-composites composed of an organic polymer matrix with dispersed inorganic nanofillers are a novel class of nano-hybrids that have many developed functional properties. These include dielectric properties, thermal stability, mechanical strength, flexibility, ductility, and processability when compared to traditional composites [1, 2]. These nanofillers, even at very low concentrations, can influence the macroscopic properties of the polymer matrix significantly [3]. This inspiring results are mainly caused by the exfoliated structure and layer intercalation of nano-fillers, which can improve the interfacial contact efficiently between the organic matrices and inorganic fillers and thus promote the properties of nano-composites. In addition, the crystallinity of polymeric matrix may be affected by the addition of nano-fillers [4].

Therefore, nano-composites can be utilized widely in various fields by adjusting different contents of nano-fillers [4, 5].

Polyimides have various applications in printed circuits, as well as in the automobile, aerospace, and memory industries due to their thermal stability, high chemical resistance, high mechanical strength, and lower dielectric constants [6–8]. Polyimides (PIs) are step or condensation polymers derived from either aliphatic or aromatic dianhydrides and diamines and their derivatives, and they contain a heterocyclic imide linkage in their repeat unit [6, 9]. The chemical composition and chain structure of PIs lead them to be infusible within the processing temperature and insoluble in organic solvents. However, the application of PIs in some fields remains limited [10]. Previous researches showed that bulky groups of PIs indeed enhanced the interchain spacing, solubility, and further prevented the coplanar phenomenon of aromatic rings [6, 11]. It is worth mentioning that most of the poly(urea-imide)s presented an excellent solubility in polar aprotic solvents such as N-methyl-2-pyrrolidone (NMP), N, N-dimethylformamide (DMF), N,N-dimethylacetamide (DMAc), and dimethyl sulfoxide (DMSO), they were partially soluble in *m*-cresol and pyridine, and they were not soluble in less polar solvents, such as chloroform ($CClH_3$) and tetrahydrofuran (THF) at room temperature. The resulting poly(urea-imide)s showed a better solubility in common organic solvents than polyimides, poly(amide-imide)s, and even poly(ether-imide)s with the same aromatic structure [10].

Smectite clays have a sandwich structure and are full of positive ion such as Na^+, Ca^{2+}, and Mg^{2+} [12, 13]. When other cations separate the clay layers, the interlamellar space will increase and allow different adsorbents and catalysts into the interlayer region and affect the pore size. For example, it can be introduced directly into the interlayer of the layered phase without pre-swelling, allowing the intercalation of the amine and pillar precursor tetramethyloxysilane (TEOS) into the interlayer [14]. The main method of TEOS intercalation between clay layers is via the sol–gel method [14, 15]. The advantages of the sol–gel method include the low reaction temperature (below room temperature) such that it cannot deposit at high temperatures, the reduced cost, and the particle size can be easily controlled by adjusting the catalyst, water, and temperature [16]. Therefore, the sol–gel technique is widely used in the preparation of uniform nano-materials from a homogeneous dispersion and can also reinforce the mechanical properties of the organic materials. The most utilized alkoxides are tetramethyloxysilane (TMOS), and tetramethyloxysilane(TEOS) [17, 18].

Porous nano-silica-pillared clay materials are characterized by a high surface area, pore volume and thermal stability [15, 19–22]. These porous nano-silica-pillared clays have received considerable attention because of their good environmental compatibility, low cost, wide availability, and they can even be reused. However, owing to the re-stacking phenomenon of nano-silica-pillared layered clays after exfoliation, the poor stability of nano-silica-pillared layered clays still restricts their development. In order to solve afore-mentioned problem, the porous nano-silica-pillared layered clays were modified by TEOS in this study. The stability of nano-silica-pillared layered clays could be improved significantly after exfoliation. In addition, the poly(urea-imide) was blended with porous nano-silica-pillared layered clays to form the nanocomposite. The properties including thermal properties, microstructure morphology, dielectric constant, and mechanical properties were investigated. The poly(urea-imide) was prepared from an aromatic diamine (4,4′-diphenylmethane diisocyanate), aromatic dianhydride (pyromellitic diahydride) and 4,4′-oxydianiline (ODA). The successful preparation of the poly(urea-imide) was confirmed by Fourier transform infrared (FTIR) spectroscopy. Different ratios of the nano-silica-pillared layered clays (NSP7030) were modified using TEOS via a sol–gel process, and the TEOS modified NSP7030 clays (NSP7030/TEOS) were further calcined at 500 °C (C-NSP7030/TEOS) and evaluated using X-ray diffraction (XRD), surface area measurements and transmission electron microscopy (TEM). Finally, the nano-hybrid composites comprising the C-NSP7030/TEOS clays and poly(urea-imide) were characterized using thermogravimetric analysis (TGA), scanning electron microscopy (SEM), and their mechanical and electrical properties examined.

Experimental

Materials

Sodium montmorillonite (Na^+-MMT), a layered silicate clay with a cationic exchange capacity (CEC) of 120 mequiv/100 g, was supplied by Nanocor Co., USA. Diethylene glycolamine ($HOCH_2CH_2OCH_2CH_2NH_2$) was purchased from Aldrich Chemical Co. The tetraethoxysilane (TEOS, ACROS Co., USA) was used as received. The 4,4′-diphenylmethane diisocyanate (MDI, ACROS Co., USA) was purified by vacuum distillation before use. The pyromellitic diahydride (PMDA, ACROS Co., USA) was purified by acetic anhydride before use. The 4,4′-oxydianiline (ODA, TCI Co., Japan) was purified by recrystallization from ethanol and dried in an oven at 110 °C for 5 h before use. All other solvents and hydrochloric acid (HCl) were purchased from ACROS Co., USA.

Silica-pillared layered clay

The nano-silica-pillared layered clays (NSP7030:70 clay/30 colloid silica) were synthesized as described in the references with minor modifications [23, 24]. In brief, the preparation of random nano-silica-pillared (NSP) layered clays were made from the intercalation of 70 wt% sodium montmorillonite (Na^+-MMT) using diethylene glycolamine. 30 wt% colloidal silica was then added to enhance the intercalation/exfoliation degree, and the average colloidal silica diameter is

approximately 100 nm. The silica-pillared layered clays (NSP7030) were isolated by toluene/NaOH phase extraction several times to remove the organic amines. The NSP7030 clays were dispersible in methanol/water at 60 °C and settled into two layers on the addition of toluene. The aqueous phase containing the silica-pillared layered clays suspension were separated and purified. The synthetic pathway and a schematic of the product structure are shown in Fig. 1a.

TEOS modified nano-silica-pillared layered clays

The NSP7030 clays were further modified by a sol–gel reaction using TEOS at different weight ratios of clay to TEOS. In a typical procedure, 2.0 g of NSP7030 clay was dispersed in 13 ml of water and stirred at 100 °C for 24 h to pre-swell the clay. Thereafter, TEOS in an ethanol solution (10 ml) was then added, and the mixture stirred for 30 min. The amount of TEOS used was 1, 3, and 5 times that of clay, which is indicated by the TEOS content of 2.0, 6.0, and 10.0 g, respectively. The TEOS/ethanol solution was then added drop wise into the pre-swelling clay solution, followed by the addition of 0.01 N HCl before the reaction mixture was refluxed at 100 °C for 3 days. The suspension was washed and collected via centrifugation, and the modified clays (NSP7030/TEOS) were dried at 200 °C for 12 h. In order to enhance the surface area of clay, 500 °C of calcination was undertaken to remove the excess organic reagents. The expected structure of NSP7030/TEOS is shown schematically in Fig. 1b.

Preparation of poly(urea-imide) and their nano-hybrid composites

This procedure used to synthesize the poly(urea-imide) by a polycondensation reaction is shown in Scheme 1. First, a 100 ml round-bottom flask equipped with a magnetic stirrer bar was charged with the diisocynanate monomer (MDI), which was then dissolved in 30 ml of dimethylacetamide (DMAc) under a nitrogen atmosphere. The dianhydride monomer (PMDA) was then added to the MDI solution and vigorously stirred at ambient temperature under N_2 for 2 h.

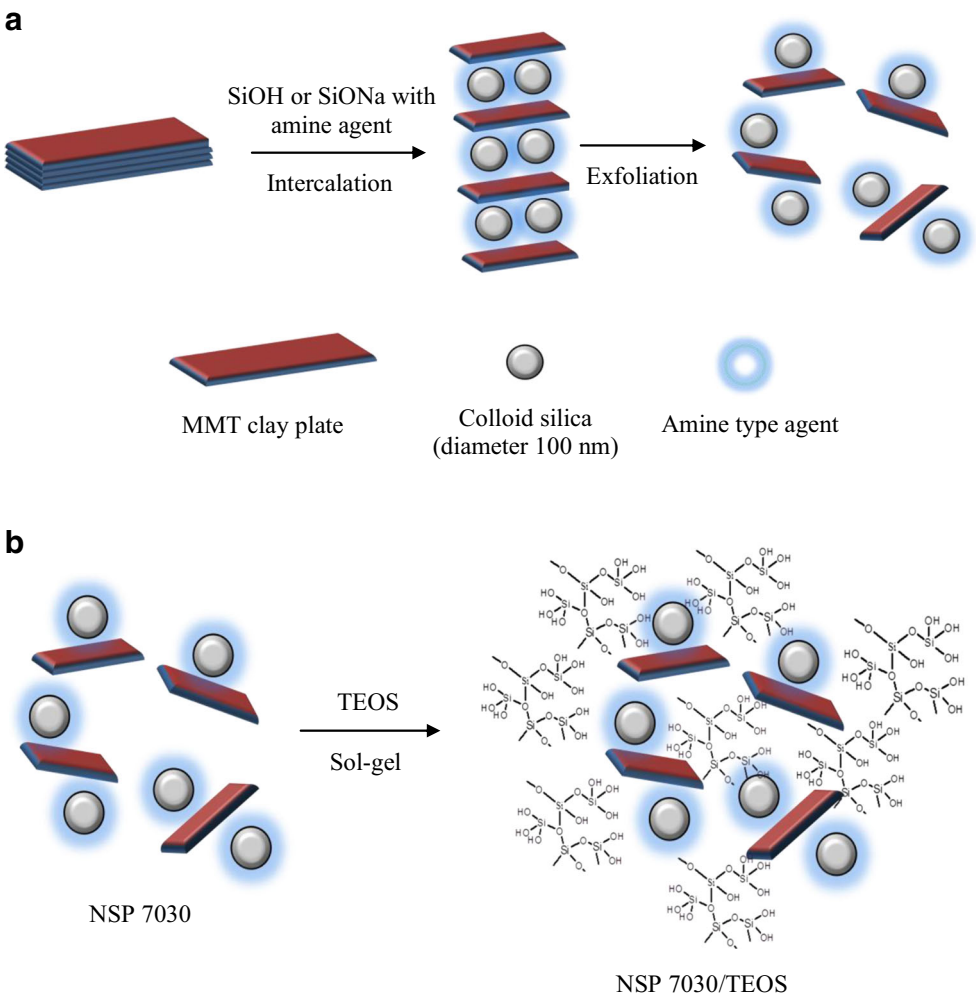

Fig. 1 Schematic diagram of **a** the synthetic pathway and the structure of the nano-silica-pillared layered clay (NSP7030) and **b** the porous nano-silica-pillared layered clay (NSP7030) modified by TEOS

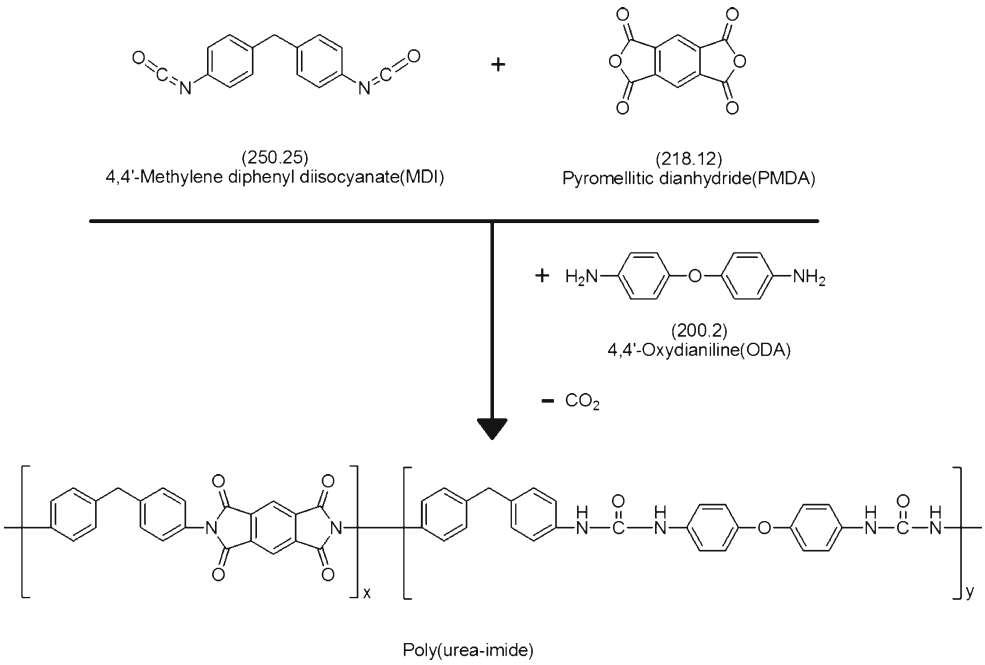

Scheme 1 Synthesis of poly(urea-imide) (PUI) from 4,4′-diphenylmethane diisocyanate (MDI), pyromellitic diahydride (PMDA) and 4,4′-oxydianiline (ODA)

Then, 4,4′-oxydianiline (ODA) was added to the homogeneous MDI/PMDA solution and stirred at room temperature until ODA was completely dissolved. The obtained solutions were pulled to a petri dish, and then putted into a vacuum oven to form the poly(urea-imide) films via a four-step process (raised the temperature to 60, 90, 120, and 200 °C step by step). The above-mentioned process was able to make the film smooth and ensure that the solvent DMAc (b.p. 167 °C) was removed completely.

The nano-hybrids comprised of poly(urea-imide) and porous silica-pillared layered clay were prepared via ultrasonic blending. Briefly, the porous silica-pillared layered clays were added into DMAc and mixed evenly under sonication. The amount of porous silica-pillared layered clay used was 5, 10, and 15 wt%, respectively. The MDI / PMDA / ODA DMAc solution was then added into the former suspension containing the porous silica-pillared layered clay, and stirred vigorously to ensure the clay was evenly dispersed. For the nano-hybrid composite samples, the mixed slurries were cast onto a petri dish, and then placed into a vacuum oven to form the nano-hybrid polymer films via a four-step process (raised the temperature to 60, 90, 120, and 200 °C step by step).

Characterization analysis

The crystallinity of the modified clays (NSP7030/TEOS) at different weight ratios of clay to TEOS were evaluated by a X-ray diffractometer using CuKα radiation (XRD; Rigaku, RINT2000, Japan). A scanning rate of 0.3°/min was used with a 2θ ranging from 2 to 10°. The microstructure was examined by transmission electron microscopy (TEM) and scanning electron microscopy (SEM). TEM observations were obtained using a JOEL JEM-1230 electron microscope operating at 100 kV. The samples were prepared by dropping the sample solution onto a copper grid coated with a carbon film. SEM was performed on a JEOL JSM-5600 system operated at 15 kV. The samples were prepared by spreading them onto a glass plate surface and evaporating to dryness in an oven at 200 °C for 8 h. The samples were coated with Pt before the SEM measurements.

Fourier transform infrared (FTIR) spectra were recorded on a Nicolet 750 spectrometer. The spectra were obtained by averaging 64 scans at a resolution of 2 cm^{-1} over a range of 500–4000 cm^{-1}. Thermogravimetric analysis (TGA) was performed using a Perkin-Elmer Pyris 1 TGA thermogravimetric analyzer at a heating rate of 10 °C/min from 100 to 800 °C under a N_2 atm. Gas adsorption analysis is commonly used for surface area and porosity measurements. Nitrogen gas is generally employed as the probe molecule and is exposed to the solid under investigation under liquid nitrogen conditions (i.e., 77 K). The Brunauer, Emmett and Teller (BET) technique is the most common method for determining the surface area of powders and porous materials [25]. Therefore, the N_2 isotherms were measured using a Micromeritics ASAP 2010 system and the surface area and pore size distribution were determined by BET analysis. The samples loading ranged from 0.4 to 0.8 g and the BET instrument was normalized by the comparison with a control group to calculate the data.

The mechanical properties were elucidated using a TIEN SHIANG Ltd., PT-166 tensile tester, and the testing method used was in accordance to ASTM D882. The dielectric constant (k) of polymer films (~100 nm) were measured by the parallel-plate capacitor method with a Precision LCR (Inductance Capacitance Resistance) Dielectric Meter (Agilent 4284A) using 1 MHz as frequency at room temperature. The dielectric constant was

calculated by the following equation: $k=Cd/\varepsilon_0 A$, where C was the capacitance, d was the film thickness, ε_0 was the permittivity of free space, A was the area of the gold electrodes. Gold electrodes were deposited onto the film surface under the vacuum environment, and the value of capacitance was measured at 25 °C and 0 % relative humidity in a sealed chamber.

Results and discussion

XRD analysis of the NSP7030 clays and the NSP7030/TEOS modified clay

The X-ray diffraction patterns of NSP7030 clay and NSP7030/TEOS are shown in Fig. 2. The XRD results showed the characteristic peak (d_{001}=1.47 nm) of the NSP7030 clay at a 2θ of 6.0°. The characteristic peak (d_{001}=1.47 nm) of the NSP7030 clay becomes smooth and broadens after the TEOS modification. More importantly, the distance between the lattice layers has increased due to layer intercalation or the exfoliated structure. For example, the modified ratio of NSP 7030/TEOS is 1/1, and the characteristic peak is shifted to a 2θ of 5.7° (d_{001}=1.55 nm). Furthermore, when the modified ratio of NSP7030/TEOS are from 1/3 to 1/5, the characteristic peak almost vanishes, which means that the amorphous phase increased after the TEOS modification. These results indicate that the TEOS has been successfully inserted into the clay to form an intercalated structure, but that an exfoliated structure has also been formed.

Gas adsorption/BET analysis of the NSP7030 clays and the NSP7030/TEOS modified clay

To follow the change in pore volume, the average pore diameter, and the surface area after calcination at 500 °C of these clays, the gas adsorption and BET were evaluated. The total pore volume, average diameter and surface area of the NSP7030 clays and the NSP7030/TEOS modified clay are shown in Table 1. The total pore volume, average pore diameter and surface area obtained for the NSP7030 clay were 0.054 cm^3/g, 181.12 Å and 12.92 m^2/g, respectively. However, for NSP7030 clay, the total pore volume (0.072 cm^3/g) and surface area (16.30 m^2/g) showed a tendency to increase with the calcination treatment at 500 °C, while the average pore diameter decreased (176.31 Å). This situation arises because the organic reagent and absorbed solvent were removed, which leads to an increase in the pore volume and surface area. However, these clay particles are denser and reduced after calcination at 500 °C, resulting in a decrease in the pore diameter size.

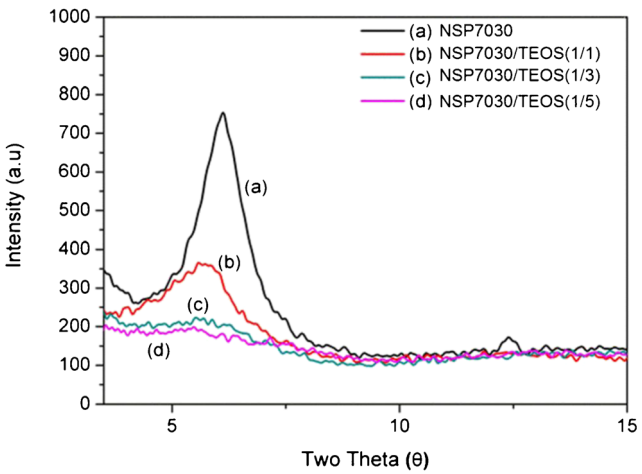

Fig. 2 XRD of the different ratio nano-silica-pillared layered clays (NSP7030) modified by tetraethyl orthosilicate (TEOS)

Furthermore, the total pore volume and surface area of the NSP7030/TEOS modified clay were increased from the NSP7030 clay, as shown in Table 2. This result is because the TEOS intercalated into the interlamellar space of clay, which enlarged the distance between the exfoliated structures. Therefore, the NSP7030/TEOS modified clay exhibits an increased pore volume and surface area compared to the NSP7030 clay. The total pore volume increased from 0.054 to 0.439 cm^3/g, and the surface area increased from 12.92 to 335.69 m^2/g for the modified ratios (1/0~1/5) of the NSP7030/TEOS modified clay. On the contrary, the average pore diameter decreased from 181.12 to 50.85 Å for the modified ratios (1/0~1/5) of the NSP7030/TEOS modified clay. This may be because the TEOS intercalated into the interlamellar space of the clay, but the loose exfoliated structure was also filled with TEOS to reduce the average pore diameter.

For the NSP7030/TEOS modified clay, the change in pore volume, average pore diameter, and surface area after calcination at 500 °C varies from the NSP7030 clay. The surface area (102.76~295.02 m^2/g) showed a tendency to decrease with the calcination at 500 °C for the NSP7030/TEOS modified clay than without calcination. However, the total pore volume (0.256~0.463 cm^3/g) and the average pore diameter (99.35 to 52.00 Å) of the NSP7030/TEOS modified clay showed a increasing tendency from the one after calcination to the one without calcination. In other words, these organic reagents and absorbed solvents could be removed to increase the pore volume and pore diameter after calcination at 500 °C in NSP7030/TEOS. At the same time, owing to the increased diameter and volume of pore, the total surface area would decrease after the calcination at 500 °C. The above results showed that remove of organic reagents influence the pore size, pore volume, and surface area of treated clay obviously.

TEM observations of the NSP7030 clays and the NSP7030/TEOS modified clay

The morphology of the exfoliated structure of the silica-pillared layered clay of the NSP7030 clay, the NSP7030/

Table 1 The total pore volume, average pore diameter, and surface area of the nano-silica-pillared layered clays (NSP7030) and the TEOS modified NSP7030 clays

500 °C Calcination	Total pore volume (cm^3/g)		Average pore diameter (Å)		Surface area (m^2/g)	
	Before	After	Before	After	Before	After
NSP7030	0.054	0.072	181.12	176.31	12.92	16.30
NSP7030/TEOS(1/1)	0.240	0.256	64.92	99.35	149.35	102.76
NSP7030/TEOS(1/3)	0.372	0.379	52.37	62.91	293.91	291.20
NSP7030/TEOS(1/5)	0.439	0.463	50.85	52.00	335.69	295.02

TEOS(1/5) modified clay, and the NSP7030/TEOS(1/5) modified clay calcined at 500 °C were investigated through transmission electron microscopy (TEM), as shown in Fig. 3. For example, the TEM image of the silica-pillared layered clay of NSP7030 showed an intercalated structure morphology, as shown in Fig. 3a. The dispersion of colloidal silica into the sodium montmorillonite (Na^+-MMT) was obtained and its size was approximately 100 nm, and the packing of NSP7030 is layer by layer. However, the exfoliated structures of the NSP7030 clays do not still seem obvious. Conversely, the exfoliated structures of the NSP7030/TEOS(1/5) modified clay showed a morphology of exfoliated (major) and intercalated (minor) structures, as shown in Fig. 3b. Therefore, the exfoliated structures of NSP7030 clay platelets may be considerably affected by the incorporation of TEOS. Sol–gel reactions of TEOS occurred in the intercalate layer, leading to the formation of three-dimensional networks, which may significantly affect the intercalated structures in the matrix, leading to a predominantly exfoliated clay structure. Moreover, we can see the porosity changed between the NSP7030 and NSP7030/TEOS(1/5) modified clays. For example, Fig. 3b shows that the NSP7030/TEOS(1/5) modified clays are highly porous within the matrix. From Fig. 3c, the three-dimensional networks of TEOS became loose and the pore volume also increased after the calcination of the NSP7030/TEOS(1/5) modified clays. The results indicated that the organic reagents might be removed completely, and thus induced the increase of pore volume.

FTIR analysis of the poly(urea-imide) (PUI) synthesis

A representative FTIR spectrum of PUI is shown in Fig. 4. The characteristic absorption bands of PUI are listed below. The characteristic absorption bands of the imide ring appear at approximately 1780 and 1720 cm^{-1} (imide-I), which is indicative of the asymmetrical and symmetrical C=O stretching vibration, and at 1350 (imide-II), 1078 (imide-III) and 726 cm^{-1} (imide-IV), whereas the imide-I, -III, -IV bands were assigned to the axial, transverse, and out-of-plane vibrations of the cyclic imide structure, respectively [26, 27]. The N–H stretching band of the urea was observed at approximately 3200–3350 cm^{-1}, and the C=O stretching band of the urea groups at 1676 cm^{-1}. The C=N stretching band of the benzothiazole groups appeared at 1619 cm^{-1}, and the N-H bending and C-N stretching bands at 1557 cm^{-1} could also be observed [10]. Other PUI had similar functional groups. However, the NCO peak observed near 2230 cm^{-1} disappeared, which means the reaction was complete.

Table 2 The thermal, mechanical, and electrical properties of the nano-hybrids of poly(urea-imide) with different weight ratios of C-NSP7030/TEOS(1/5)

Polymer	T_d 5 %[a] (°C)	T_d 10 %[b] (°C)	Tensile strength[c] (MPa)	Elongation (%)	K[d]
pure PUI	465	525	96.1	9.0	3.88
5 wt% C-NSP7030/TEOS(1/5)/PUI	475	530	112.7	5.1	3.62
10 wt% C-NSP7030/TEOS(1/5)/PUI	490	530	71.6	4.1	3.47
15 wt% C-NSP7030/TEOS(1/5)/PUI	510	535	43.1	2.7	3.31

The C-NSP7030/TEOS(1/5) modified clay was calcined at 500 °C

[a] Thermal decomposition temperature at 5 % weight loss

[b] Thermal decomposition temperature at 10 % weight loss

[c] Tensile strength is test by ASTM D822

[d] Dielectric constants were measured at 1 MHz and at room temperature

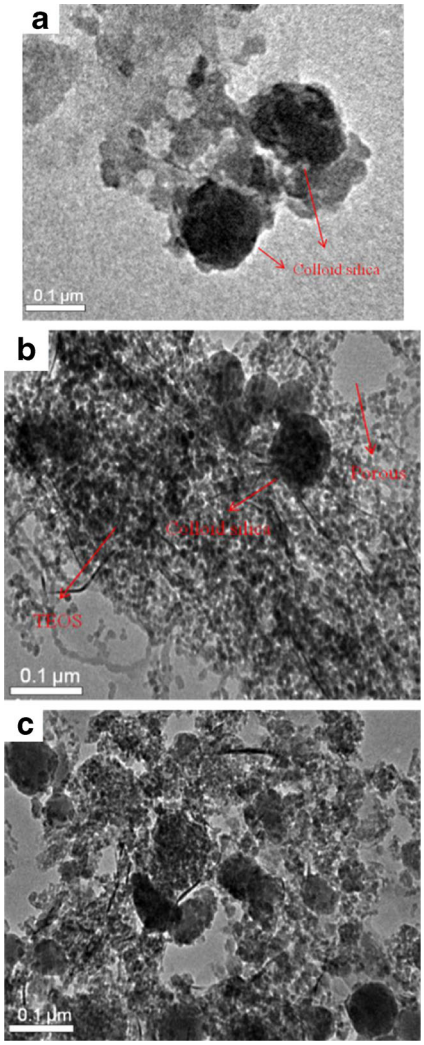

Fig. 3 TEM of the **a** silica-pillared layered clay of NSP7030, **b** NSP7030/TEOS(1/5), and **c** C-NSP7030/TEOS(1/5)

TGA analysis of the C-NSP7030/TEOS/PUI composites

The thermal properties of the resulting poly(urea-imide) and their nano-hybrids (poly(urea-imide) and C-NSP7030/TEOS(1/5) modified clays) were determined by means of thermogravimetric analysis (TGA), which are shown in Fig. 5. From the previous section, the NSP7030/TEOS(1/5) modified clay after calcination at 500 °C (C-NSP7030/TEOS(1/5)) exhibited a higher pore volume than NSP7030. As such, the nano-hybrids were that the C-NSP7030/TEOS(1/5) incorporated into the PUI polymer. The thermal behavior of these materials is summarized in Table 2. The excess addition of nano-silica-pillared layered clay was not able to disperse in the PUI matrix easily, but their thermal stabilities were almost similar to the pure PUI polymer. The obtained results indicated that the thermal properties of nano-hybrids were mainly associated with the PUI polymer structure.

The obtained PUI were stable even as the temperature was 450 °C, and their decomposition temperature at 5 wt.% and 10 wt.% lost were 465 and 525 °C approximately. On the other hand, all thermograms showed two-step thermal decomposition patterns. The maximal decomposition temperature in the first stage was approximately 340–365 °C, which corresponds to the decomposition of the urea groups [10]. The decomposition temperature in the second stage appeared at 520–550 °C approximately due to the decomposition of the imide linkages. Therefore, the 10 % weight loss temperatures arise from the decomposition of ureylene linkages. As shown in Table 2, the PUI nano-hybrids exhibited good thermal stability compared to the pure PUI. The decomposition temperature at 5 wt.% of the PUI nano-hybrids was slightly higher than the pure PUI. These observations may be attributed to the early degradation of the urea linkages than those of the imide groups against high temperatures. The highest decomposition temperature at 5 wt.% of the PUI nano-hybrids was 510 °C as the content of C-NSP7030/TEOS(1/5) was 15 wt.%. Therefore, the thermal stability seems to be mainly the PUI molecules cleavage-based. But the interface area amount between polymer molecules and nano-clay is also able to slightly

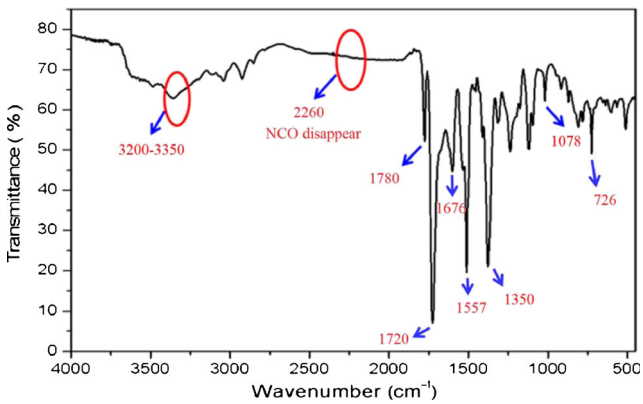

Fig. 4 FTIR spectrum of the poly(urea-imide) prepared from 4,4′-diphenylmethane diisocyanate (MDI), pyromellitic diahydride (PMDA) and 4,4′-oxydianiline (ODA)

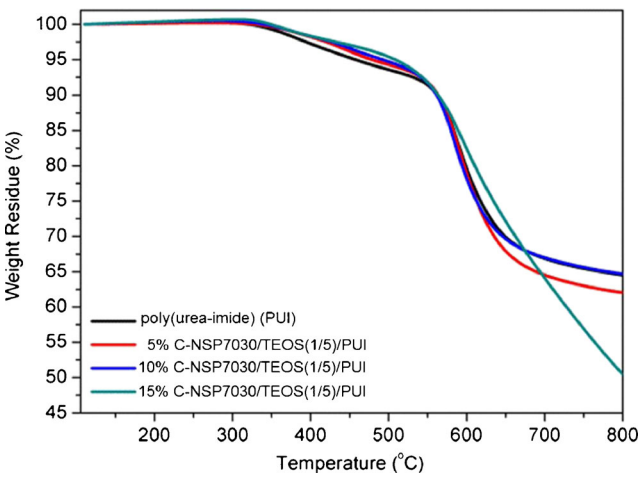

Fig. 5 TGA of the poly(urea-imide) and nano-hybrids comprising different weight ratios of the C-NSP7030/TEOS(1/5) to poly(urea-imide)

increase the T_d 5 %. However, the excess addition of nano-silica-pillared layered clay resulted in the aggregation domains, poor adhesion on the substrates, and early decomposition of nano-hybrids at 510 °C.

SEM observations of the C-NSP7030/TEOS/PUI composites

The SEM micrographs showing the effect of the C-NSP7030/TEOS(1/5) clay loading in a poly(urea-imide) matrix on the morphology of the resulting nano-hybrids are shown in Fig. 6. The micrographs in Fig. 6a and e show that the surface and cross-section morphology were smoother for the poly(urea-imide) only, respectively. The micrographs in Fig. 6b, c, and d show the surface morphologies of the nano-hybrids of poly(urea-imide) with 5, 10 and 15 wt% C-NSP7030/TEOS(1/5) clay loading, respectively. With increased nano-hybrid loading, the roughness tended to increase.

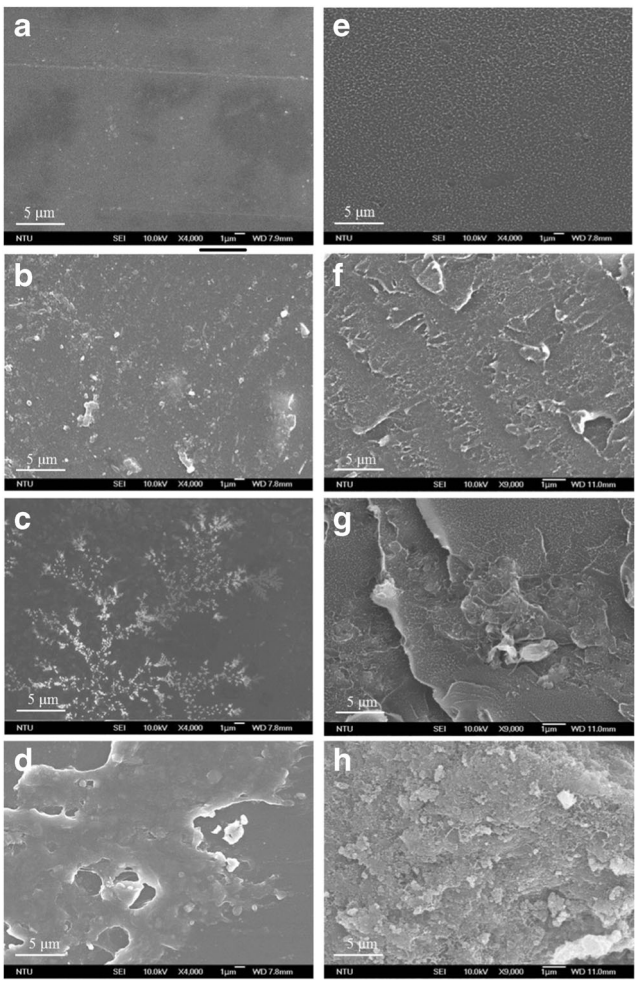

Fig. 6 SEM of the poly(urea-imide) and nano-hybrids comprising different weight ratios of the C-NSP7030/TEOS(1/5) to poly(urea-imide). The surface of **a** PUI, **b** 5 % C-NSP7030/TEOS(1/5), **c** 10 % C-NSP7030/TEOS(1/5), and **d** 15 % C-NSP7030/TEOS(1/5). The cross-section of **e** PUI, **f** 5 % C-NSP7030/TEOS(1/5), **g** 10 % C-NSP7030/TEOS(1/5), and **h** 15 % C-NSP7030/TEOS(1/5)

The fracture morphologies of the nano-hybrids of poly(urea-imide) loaded with 5, 10 and 15 wt% C-NSP7030/TEOS(1/5) clay are shown in Fig. 6f, g, and h, respectively. In Fig. 6g and h, the C-NSP7030/TEOS(1/5) clay was found to agglomerate 10, and 15 wt% of the C-NSP7030/TEOS(1/5) clays were loaded into the PUI matrix. This result may arise because these clay nanoparticles easily agglomerate due to their large surface-to-volume ratios and high surface tension. However, at lower clay loadings, the C-NSP7030/TEOS(1/5) clay dispersed well in the PUI matrix with an optimal dosage <5 wt%, as shown in Fig. 6f.

Mechanical properties and dielectric constant analysis of the C-NSP7030/TEOS/PUI composites

Compared to the organic-functionalized clays, inorganic clays owned the rigid property, but had the problems of aggregation and poor adhesion which would influence the properties of nano-hybrid. Table 2 shows the tensile strength of the nano-hybrids of poly(urea-imide) at 5, 10 and 15 wt% C-NSP7030/TEOS(1/5) clay loading. For pure PUI, the tensile strength was 96.1 MPa. The tensile strength after the inclusion of 5, 10, and 15 wt% clay became 112.7, 71.6, 43.1 MPa, respectively. Therefore, the great improvement of mechanical properties and adhesion for hybrid materials could be achieved by dispersing nano-sized clay particles within the PUI matrix uniformly. For example, the tensile strength increased after the incorporation of 5 wt% C-NSP7030/TEOS(1/5) clay into the PUI matrix. Moreover, the higher C-NSP7030/TEOS(1/5) clay loading, the elongation at break % of the nano-hybrid composites decreases due to its brittle properties and aggregation, as shown in Table 2. For pure PUI, the elongation was 9%. After the inclusion of 5, 10, and 15 wt% clay, the elongation became 5.1, 4.1, 2.7 %. These results were also confirmed from SEM observations.

The dielectric constant, k, of these polymer films were investigated by the parallel-plate capacitor method, and the data are summarized in Table 2. The dielectric constants of the nano-hybrid composites ranged from 3.88 to 3.31. The dielectric constants decreased as a function of the C-NSP7030/TEOS(1/5) clay content. In previous reports, the dielectric properties have been designed by introducing polarizable groups into the polymer chains, increasing the free volume by inducing porosity as well as copolymerization [28]. Table 2 shows the dependence of the dielectric constant on the pore volume based on the C-NSP7030/TEOS(1/5) clay content. The pure PUI had a total pore volume of 0.072 cm^3/g. After the inclusion of 5, 10, and 15 wt% of C-NSP7030/TEOS(1/5) clays, the total pore volume was 0.256, 0.379, 0.463 cm^3/g, respectively. In other words, a higher pore volume will reduce the dielectric constant.

Conclusion

The nano-hybrids comprising poly(urea-imide) (PUI) and porous nano-silica-pillared layered clays are promising materials due to the improvement of several properties. Synthesis of PUI was confirmed by FTIR spectroscopy. The intercalation and random exfoliation of the nano-silica-pillared layered clays modified by TEOS (NSP7030/TEOS) via a sol–gel technique with an acidic solution have been achieved and were confirmed by X-ray diffraction techniques, gas adsorption, BET analysis and TEM observation. The pure PUI obtained were stable up to 450 °C and lost 5 % (T_d at 5 %), 10 % (T_d at 10 %) of their total weight at approximately 465 and 525 °C, respectively. The nano-hybrids of PUIs exhibited a slightly higher thermal stability than pure PUI. For example, the T_d 5 % was 475 °C because the nano-hybrids consisted of PUI with 5 % C-NSP7030/TEOS(1/5) clay. The mechanical results also showed that the tensile strength increased because the nano-hybrids of PUI contained 5 wt% C-NSP7030/TEOS(1/5) clay. While pure PUI exhibits a tensile strength of 96.1 MPa, after the inclusion of 5, 10, and 15 wt% C-NSP7030/TEOS(1/5), the tensile strength was 112.7, 71.6, 43.1 MPa, respectively. With increased nano-hybrid loading, the roughness tended to increase. When lower loadings of the C-NSP7030/TEOS(1/5) clay were used, the clay was well dispersed in the PUI matrix with an optimal dosage <5 wt%. In addition, the higher the C-NSP7030/TEOS(1/5) clay loading, the elongation at break % of the nano-hybrids is reduced due to its brittle properties and aggregation. The addition of C-NSP7030/TEOS(1/5) clays also increased the total pore volume and reduced the dielectric constant. Therefore, the nano-hybrids of PUIs may be used for electronic boards because of their high-temperature resistance and low dielectric constant in the future.

Acknowledgments The authors gratefully acknowledge the support for this research by the Ministry of Economic Affairs in Taiwan under the grant numbers 101-EC-17-A-08-S1-205 and Kaohsiung Medical University in Taiwan under the grant numbers KMU-TP103B03, respectively

References

1. Zou H, Wu SS, Shen J (2008) Chem Rev 108:3893–3957
2. Gilman JW, Jackson CL, Morgan AB, Jr RH (2000) Chem Mater 12:1866–1873
3. Wei LM, Tang T, Huang BT (2004) J Polym Sci Pol Chem 42:941–949
4. Bilotti E, Fischer HR, Peijs T (2008) J Appl Polym Sci 107:1116–1123
5. Natta G, Corradini P (1960) Nuovo Cim (Suppl) 15:40–51
6. Chang WY, Chen SH, Yang CH, Chuang CN, Wang CK, Hsieh KH (2015) J Polym Res 22:38–46
7. Wang L, Chang P, Cheng CL (2006) J Appl Polym Sci 100:4672–4678
8. Ghosh MK, Mittal KL (1996) Polyimides: fundamentals and applications. Marcel Dekker, New York
9. Li Y, Wang Z, Li GJ, Ding MX, Yan JL (2012) J Polym Res 19: 9772–9778
10. Toiserkani H (2011) Open J Polym Chem 1:1–9
11. Yang CP, Chen WT (1993) Macromolecules 26:4865–4871
12. Reichle WT, Kang SY, Everhart DS (1986) J Catal 101:352–359
13. Depege C, El Metoui FE, Forano C, de Roy A, Dupuis J, Besse JP (1996) Chem Mater 8:952–960
14. Qian Z, Hu G, Zhang S, Yang M (2008) Phys B Condens Matter 403:3231–3238
15. Mao H, Li B, Yue L, Wang L, Yang J, Gao X (2011) Appl Clay Sci 53:676–683
16. Matijević E (1994) Langmuir 10:8–16
17. Letaïef S, Martín-Luengo MA, Aranda P, Ruiz-Hitzky E (2006) Adv Funct Mater 16:401–409
18. Letaief S, Ruiz-Hitzky E (2003) Chem Commun 24:2996–2997
19. Moini A, Pinnavaia TJ (1986) Solid State Ionics 26:119–123
20. Kwon OY, Park KW, Jeong SY (2001) Bull Korean Chem Soc 22: 678–684
21. Nakao T, Nogami M (2005) Mater Lett 59:3221–3225
22. Zhou, Li X, Ge Z, Li Q, Tong D (2004) Catal Today 93–95:607–613
23. Chu CC, Chiang ML, Tsai CM, Lin JJ (2005) Macromolecules 38: 6240–6243
24. Chiu CW, Chu CC, Dai SA, Lin JJ (2008) J Phys Chem C 112: 17940–17944
25. Brunauer S, Emmett PH, Teller E (1938) J Am Chem Soc 60:309–319
26. Toiserkani H, Sheibani H, Saidi K (2011) Polym Adv Technol 22: 1494–1501
27. Toiserkani H (2011) High Perform Polym 23:542–554
28. Hung TV, Frank GS (2002) Microelec J 33:409–415